Acoustic developments for the measurement of sediment processes over bedforms

Peter D. Thorne [(1)]

1. National Oceanography Centre, Liverpool, UK - pdt@noc.ac.uk

Abstract

The processes of near bed sediment dynamics involves feedback mechanisms, with the hydrodynamics, bedforms and sediment transport each mutually interacting and modifying one another. To understand these interactions requires co-located, simultaneous, high temporal-spatial resolution measurements of the three components of this interacting sediment triad. To study the triad, acoustics has been increasingly utilised over the past two decades. The development and application of acoustic systems capable of measuring near bed hydrodynamics, suspended sediments, bedload and bedforms is now contributing significantly to the measurement of sediment transport processes. Here we look at the application of these acoustic techniques to the study of sediment transport in large scale wave flume facilities and present results on sediment dynamics over sandy rippled beds under waves.

1. INTRODUCTION

To predict sediment transport requires a detailed understanding of the fundamental physical processes that lead to the movement of sediments. The processes can be thought of as dynamic interactions with feedback between: (i) the seabed morphology; (ii) the sediment field; and (iii) the hydrodynamics. This process has been coined the 'Sediment triad'.

The vision two to three decades ago was that acoustics may provide simultaneous measurements of all three components of the sediment triad. Acoustics was considered to have the potential to measure non-intrusively, with high temporal-spatial resolution, co-located profiles of suspended sediment particle size, concentration, the three orthogonal components of flow and bedforms, at intra-wave, intra-ripple and turbulent scales.

Here we look at the application of acoustics to sediment transport processes (Huther et al 2011) and illustrate its use through a study on sediment diffusivity (Thorne et al 2009)

2. ACOUSTIC INSTRUMENTS

2.1 Acoustic backscatter systems, ABS

As illustrated in figure 1 Multi-frequency ABS are used to measure near bed vertical profiles of suspended particle size and concentration, usually over the bottom 1-2 m above the bed with centimetric/millimetric spatial resolution and sub-second temporal resolution.

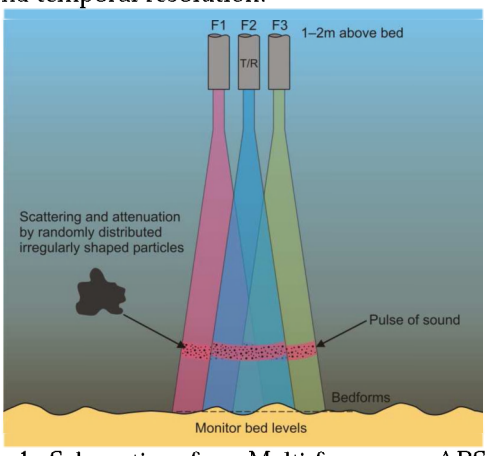

Figure1 Schematic of a Multi-frequency ABS for measuring vertical profiles of suspended particle size and concentration.

Using a combination of theoretical inversions (Thorne et al 2011), formulations for the scattering properties of natural irregularly shaped non-cohesive sediments (Moate and Thorne 2012) and exploiting the differential scattering characteristics with size and frequency, quantitative measurements of suspended sediment profiles can be obtained (O'Hara Murray et al 2012). Also because the echo from the bed is included in the acoustic backscattered signal the suspended sediment profiles can be referenced to the bed location.

To illustrate the type of measurements obtained from an ABS, figure 2 shows measurements of suspended sediments under waves over a vortex rippled sandy bed. The figure shows a high concentration even on the leeside of the ripple associated with the formation of a vortex, entraining and trapping sediments which was ejected over the ripple crest at flow reversal and up into the water column.

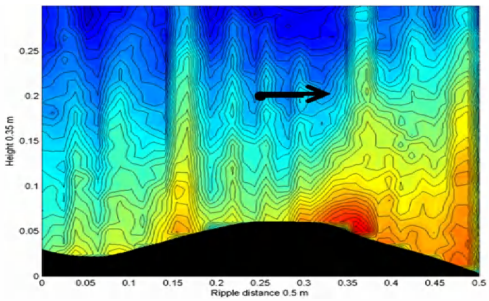

Figure 2. ABS image of suspended sediment entrainment over a vortex sand ripple under waves, with the arrow showing the instantaneous direction of flow.

2.2 Acoustic ripple profiles, ARP

As indicated above, bedforms impact on sediment transport processes and therefore it is essential to measure the features on the bed. Imaging from high frequency acoustic sector scanners has been around for a number of years (Hay and Wilson 1994). More recently two and three dimensional ripple profilers, ARP, which provide transects of the bed and actually measure the detailed bed topography have become available in recent years (Traykovski 2007).

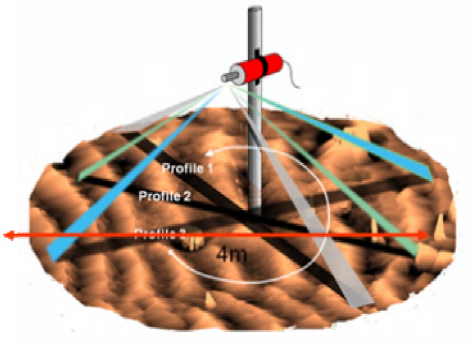

Figure 3. Illustration of a 3D-ARP covering a 4 m transect.

Figure 3 illustrates the mode of operation of a 3D-ARP. A narrow sound beam bisects a line along the bed and generates a two dimension transect of the bed providing a height profile, h(x,z). The system rotates through an angle and measures another transect. The system rotates through 180° and builds up the topography shown in figure 3. From such measurements ripple height, wavelength, orientation and migration rates can be obtained.

2.3 Acoustic Doppler velocity profilers, ADVP

Measurement of the hydrodynamics is central to any sediment transport study. For near bed studies the acoustic Doppler velocimeter, ADV, is often the instrument of choice. This provides the three orthogonal components of flow at one height above the bed. In more recent years, profiling systems, ADVP, based on the same coherent signal processing of the backscattered signal have been developed (Hurther and Lemmin 2008. Hay et al 2012). Figure 4 illustrates the arrangement.

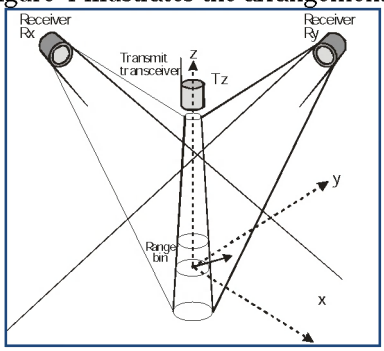

Figure 4 Schematic of an acoustic Doppler velocity profiler, ADVP

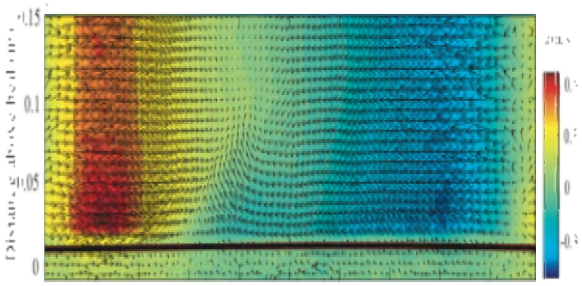

Figure 5. Vector v(u,w,z,t) flow structure during a 6.5 s wave period over a rippled bed underwaves .

Transducer Tz transmits a short pulse of sound and transducers Tz, Rx and Ry, receive the backscattered sound from sediment in suspension. Using coherent processing on the backscattered signal, high temporal-spatial profiles of the three orthogonal components of velocity can be

calculated. Figure 5 illustrates the type of measurements that can be collect. An ADVP was mounted above a rippled bed and profiles of the horizontal, u, and vertical, w, flow were collected. The vectors and colours show the detailed flow over a wave period at one location above a rippled bed.

3. ACOUSTIC PROCESS STUDY

3.1 Sediment diffusivity

Predictions for the form of the suspended sediment concentration profile are varied, differing according to the flow regime, the seabed sediment type and the bedforms. Most of the formulations to date have been underpinned by the classical concept of gradient diffusion (eg van der Werf et al 2006) In the simplest case the time averaged vertical turbulent diffusive flux of sediment, q_v, is considered to be balanced by the settling of the suspended sediment under gravity, such that:

$$q_v = w_s C \quad \text{where} \quad q_v = -\varepsilon_s \frac{\partial C}{\partial z} \tag{1}$$

Here C is the time-averaged sediment concentration at height z above the bed, w_s is the sediment settling velocity, and ε_s is the sediment diffusivity.

Despite the wide use of gradient diffusion, several studies (eg O'Hara Murray et al 2011) have indicated that this is not always the dominant process generating the suspended sediment concentration profile, particularly for sediment entrainment by waves over steeply rippled beds with $\eta_r/\lambda_r \geq 0.12$, where η_r is the ripple height and λ_r is the ripple wavelength. The mixing close to the bed is then dominated by a coherent process involving boundary layer separation on the lee-side of the ripple crest during each wave half-cycle near maximum flow velocity. The resulting lee-wake vortex remains attached to the bed entraining sediment into the flow as it grows in size and strength. At flow reversal the sediment-laden vortex is ejected into the water column, carrying sediment to several ripple heights above the bed. This process is coherent and repeatable and thus fundamentally different from that associated with gradient diffusion.

3.2 Sediment diffusivity models

Three diffusivity models are investigated. i) Nielsen's (1992) wave-averaged sediment diffusivity for rough and rippled bed is given by

$$\varepsilon_s = 0.016 k_s U_o \tag{2}$$

where U_o is the near-bed velocity amplitude and $k_s = 25\eta_r(\eta_r/\lambda_r)$ is the equivalent bed roughness. ii) The formulation of Van Rijn (1993) is expressed as

$$\varepsilon_{s1} = \alpha_b k_s U_o \qquad z \leq \zeta_s \tag{3(a)}$$

$$\varepsilon_{s2} = \alpha_m \frac{Hh}{T} \qquad z \geq 0.5h \tag{3(b)}$$

$$\varepsilon_{s3} = \varepsilon_{s1} + (\varepsilon_{s2} - \varepsilon_{s1})\left[\frac{z - \zeta_s}{0.5h - \zeta_s}\right] \qquad \zeta_s < z < 0.5h \tag{3(c)}$$

Here ε_{s1} and ε_{s2} are, respectively, constant values for the sediment diffusivity near the bed and in the upper half of the water column, with the latter value being the larger; ζ_s is the thickness of the near-bed mixing layer and h is the water depth. In this present study the expression $\zeta_s = k_s$ $(=25\eta_r(\eta_r/\lambda_r))$ has been adopted for ease of comparison with Nielsen's formulation. Coefficient $\alpha_b = 0.004D_*$, where D_* is the dimensionless grain size , H is the wave height, T is the wave period and the coefficient $\alpha_m = 0.035$. iii) The form often used for the sediment diffusivity is a simple linear increase in ε_s with height above the bed. This is commonly expressed as

$$\varepsilon_s = \beta \kappa \bar{u}_* z \tag{4}$$

where $\kappa = 0.4$ is Von Karman's constant. Here the mean magnitude of the friction velocity, $\bar{u}_*$, over the wave cycle is used to be representative of the turbulent mixing during the wave cycle as a whole.

$$\bar{u}_* = 0.763(f_w/2)^{0.5} U_o \quad , \quad f_w = 0.237\left(\frac{k_s}{A_o}\right)^{0.52} \tag{5}$$

where f_w is the friction factor formulated by Soulsby (1997).

3.3 Acoustic and auxiliary measurements

The study was conducted in the Deltaflume of the Netherlands. The large size of this flume, 240 m in length, 5 m in width and 7 m deep, allow hydrodynamic and sediment transport to be studied at full scale. The experiments were conducted beneath weakly-asymmetrical, regular, surface

waves with heights, H, and periods, T, in the respective ranges H=0.6-1.1 m and T=4–6 s over medium sand and H=0.5-1.1 m and T=4–5 s over fine sand. The medium sand had d_{50}=330 μm and the fine sand had d_{50}=160 μm; both the sands were reasonably well sorted.

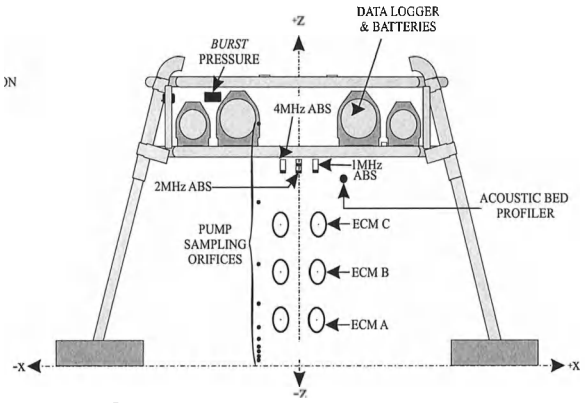

Figure 6 Schematic of the instrumented tripod used for the measurements. Shown is the triple frequency acoustic backscatter system, ABS, the acoustic ripple profiler, ARP, the pumped sampling heights and the electromagnetic current meters, ECMs.

Figure 6 shows the instrumented tripod platform used to collect the measurements. The main acoustic instruments relevant to the study were an ABS and a 2D-ARP. Auxiliary measurements using pumped sampling and electromagnetic current meters, ECMs, were collected.

High-resolution vertical profiles of the suspended sediments were measured using a triple-frequency ABS. The ABS provided 128 backscatter profiles each second, at each of the three frequencies, 1 MHz, 2 MHz and 4 MHz. Each profile consisted of 128 range bins, with a spatial resolution of 0.01 m, thereby covering a range of 1.28 m. Physical samples of the suspension were obtained by pumping through nozzles located at ten heights above the bed between 0.053 and 1.55 m. The samples were used to calibrate and assess the veracity of the acoustic backscatter measurements and provide profiles of w_s. To establish whether ripples were present on the bed, and to monitor their evolution and migration, a 2D-ARP, was used. The ARP operated at 2.0 MHz, and provided sub-centimetric measurements of the bed location over a 3m transect along the direction of wave propagation. Three ECMs located at 0.3, 0.6 and 0.91 m above the bed provided measurements of the along-flume and vertical components of the flow velocity at 8 Hz.

The measured ABS concentration profiles and w_s determined from the d_{50s} particle size profile from the pumped sample data, were used to calculate the sediment diffusivities ε_s with

$$\varepsilon_s = \frac{-w_s C}{dC/dz} \tag{6}$$

w_s is given by Soulsby (1997) as:

$$w_s = \frac{\nu}{d_{50s}}\left[(10.36^2 + 1.049D_*^3)^{0.5} - 10.36\right] \tag{7}$$

To compare results from all the different experiments the resulting sediment diffusivity profiles were normalised by plotting the parameters z/k_s and $\varepsilon_s/U_o k_s$.

3.4 Analysis and interpretation

Medium sand case. Using equation (6)and (7), ε_s was calculated from the ABS concentration profiles and the pumped sample particle size profiles. The results for the 39 sediment diffusivity profiles, from the 13 experiments were normalization and averaged to obtain the profile shown by the large solid circles with error bars in figure 7a. The data show approximately constant normalised sediment diffusivity in the region below $z/k_s \approx 1.3$. At heights greater than $z/k_s \approx 1.3$, $\varepsilon_s/U_o k_s$ increases linearly.

Using equation (2), Nielsen's empirical prediction for the constant normalized sediment diffusivity was calculated. This is shown by the dotted line in figure 7a and has a value of 0.016. This prediction is somewhat less than the presently measured value of 0.029. Considering the Van Rijn formulation for the constant sediment diffusivity layer, the value predicted by equations (3a) is 0.028, which is close to the measured value obtained here. Using equation (3a-3c) the predicted linear portion of the normalized sediment diffusivity does not result in a single curve for the present normalization. Therefore, rather than showing the calculations for each case, the bounds from the calculations are given by the two dashed lines. Given the limited data upon which equations (3a-3c) were based, the predictions are considered to be in reasonable agreement with the present data.

To complete the comparison of predictions with observations, equation (4) has been evaluated

using equation (5), and the result has then been normalised to yield

$$\frac{\varepsilon_s}{k_s U_o} = 0.763\kappa\beta\sqrt{\frac{f_w}{2}}\frac{z}{k_s} \qquad (8)$$

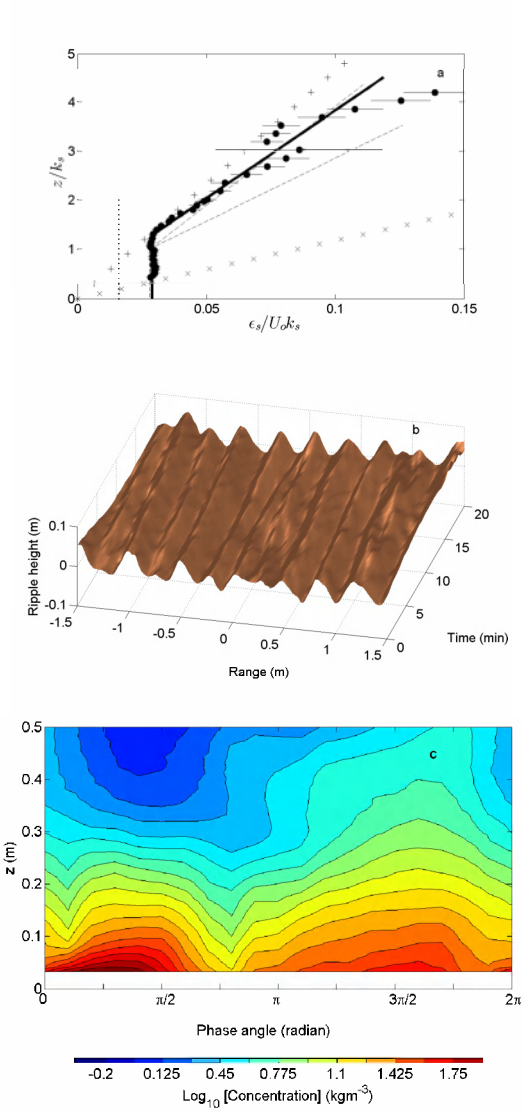

Figure 7. Comparison of the mean measured normalised sediment diffusivity (•) over the medium sand bed, with the calculations from equations (2) (····), (3) (----), (8) (x,+, see text) and (9) (▬). b) A transect of the bed over time for an experimental run with H=0.81 m and T= 5s and c) variation in concentration with the phase of the wave and height above the bed for the medium sand.

If equation (8) is evaluated using a mean value for f_w, from all the medium sand experiments, calculated using $k_s=25\eta_r(\eta_r/\lambda_r)$ in equation (5) and with $\beta=1$, the predictions for the sediment diffusivity ('×') substantially overestimate the observed values in the linear region. However, if f_w is calculated using a flat bed approximation $k_s=2.5d_{50}$ based on the grain size, then equation (8), again with $\beta=1$, yields the line in figure 7a represented by the '+' symbols. Evidently this latter outcome compares favourably with the data in the linear region

Finally, in order to capture the behaviour of the diffusivity in this case involving the medium sand, simple expressions have been fitted to the present data set to yield empirical expressions for the variation of sediment diffusivity with height above the bed. These expressions are as follows:

$$\varepsilon_s = \xi_1 U_o k_s \qquad z \leq 1.3k_s \qquad (9a)$$

$$\varepsilon_s = \xi_2 U_o z - \xi_3 U_o k_s \qquad z \geq 1.3k_s \qquad (9b)$$

where $\xi_1=0.029$, $\xi_2=0.028$, $\xi_3=0.007$ and the expression is given by the solid line in figure 7a. Further studies are required to assess the general applicability of equation (9)

To investigate the processes underlying the form of the sediment diffusivity profile, both the bedforms and the variation of suspended sediment concentration with the phase of the wave and height above the bed were examined. To illustrate the type of bedforms present on the medium sand, a typical measurement from the ARP is shown in figure 7b. The plot shows the development of a transect, over a 17 min period, for the case of T=5 s and H=0.81 m. The ripples were well developed with dimensions of $\lambda_r=0.34$ m, $\eta_r=0.047$ m, and slope of $\eta_r/\lambda_r=0.14$. This was typical for the medium sand, with $\langle\eta_r\rangle=0.05\pm0.01$ m, $\langle\lambda_r\rangle=0.36\pm0.07$ m, $\langle\eta_r/\lambda_r\rangle=0.14\pm0.01$ and $\langle k_s\rangle=0.17\pm0.03$ m, where $\langle\ \rangle$ represents an average over all experiments. The value for k_s is quite large indicating that the bed is having a major impact on the near-bed flow. To assess the mechanisms of sediment entrainment directly over the medium sand, intra-wave processes were investigated. The results are shown in figure 7c; here the intra-wave height variation of the ripple-averaged suspended sediment concentration, has been constructed over the 17 min recording period. It can be seen clearly that there are two main entrainment events and that these occur close to flow reversal ($\pi/2$, $3\pi/2$). Further analysis of this

data (Davies and Thorne 2005, Thorne et al 2009) supported the concept that the observations shown in figure 7c can be interpreted as arising from flow separation on the lee slope of the ripple, with the consequent generation of growing lee slope vortices. The processes are not random, but are repeatable and coherent. Importantly, the layer in which these effects occur may be seen to correspond to several ripple heights in thickness.
The intra-wave observations in figure 7c may be related to the sediment diffusivity profile in figure 7a in the following way. Due to the formation of vortices on the ripple lee slopes, suspended sediments were contained within a relatively fixed mixing region, of height comparable with the ripple height η_r, for most of the wave cycle. Near flow reversal the vortices were lifted up into the water column, retaining their structure to a height of the order of k_s. It is the associated coherence of sediment entrainment and structure that leads to the constant value for the sediment diffusivity within about $z/k_s \leq 1.3$ ($3\eta_r$-$4\eta_r$ for the medium sand). At heights greater than $z/k_s \approx 1.3$, the coherent structure of the vortices breaks down, with mixing of momentum increasingly becoming dominated by random turbulent processes (Ranasoma and Sleath, 1992). Here, therefore, gradient diffusion dominates and mixing increases due to an increase in the mixing length scale with height above the bed, leading to the linear increase in sediment diffusivity above the vortex layer.

Fine sand Using equation (6) and (7), ε_s was calculated for the fine sand bed, using the ABS concentration profiles together with the pumped sample particle size profiles. The normalised averaged results for the 21 sediment diffusivity profiles, from the 7 experiments are shown in figure 8a. The results show no indication of a constant diffusivity near-bed layer, but instead exhibit a sediment diffusivity that increases linearly with height above the bed. This shows no indication of a near-bed constant sediment diffusivity, associated in the medium sand measurements with vortex formation and entrainment of sediments. Instead, the results show, in the near-bed region, that the normalised sediment diffusivity increases linearly with height above the bed. Because there is no obvious constant near-bed sediment diffusivity, no useful comparison can be made with the formulations of Nielsen (Eq. (2)) or Van Rijn (Eq. (3a)). However, it is possible to compare Van Rijn's linearly increasing sediment diffusivity region with the present data. If, in equation (3c), ζ_s and ε_{s1} are set to zero, then using linear wave theory in the determination of ε_{s2} we have

$$\frac{\varepsilon_s}{k_s U_o} = \frac{2\alpha_m}{\pi} \sinh(kh) \frac{z}{k_s} \qquad (10)$$

where k is the wave number of the surface waves. Using this expression and taking the mean value of k for all the fine sand experiments, the dashed line in figure 8a is obtained. The resulting, predicted, normalised sediment diffusivity is comparable with the observed values, though it somewhat overestimates them. Reducing α_m from 0.035 to 0.022 brings Van Rijn's expression into line with the observations. Given the limited data set upon which equation (3b-3c) is based, this adjustment does not seem unreasonable. Secondly, equation (4) expressed in the form of equation (8) was compared with the data. It is interesting to note that, if equation (8) is evaluated using $k_s = 25\eta_r(\eta_r/\lambda_r)$ in equation (5), with $\beta=1$, as shown by the '×' symbols in figure 8a the predictions again significantly overestimate the observed values. However, if the flat bed approximation $k_s = 2.5d_{50}$ is used, the line in figure 8a represented by the '+' symbol is obtained, which can be seen to compare favourably with the data, with only a minor overestimation occurring. Given both these fine sand results and also those for the medium sand, it does appear to be the case that the use of $k_s = 25\eta_r(\eta_r/\lambda_r)$, for a rippled bed, overestimates the roughness length substantially if equation (4) is used to calculate ε_s.

Finally if, as in the medium sand case, an empirical fit is made to the data, forcing $\varepsilon_s = 0$ at $z=0$, then the following expression results:

$$\varepsilon_s = \chi_1 U_o z \qquad (11)$$

where $\chi_1 = 0.017$. This is comparable, though a somewhat smaller gradient than that for the linearly increasing region of the sediment diffusivity in the medium sand case.
To explain the form of the sediment diffusivity over the fine sand and its difference from the medium sand, we have again looked at the bedforms. Figure 8b shows a typical example of the ripple formation for waves with T=5 s and H=0.79 m; these inputs are very comparable with

the case shown in figure 7b for the medium sand. However, for the fine sand the ripples can be seen to be less well developed and less coherent in form, with, in the case shown, η_r=0.019 m, λ_r=0.27 m and η_r/λ_r=0.07.

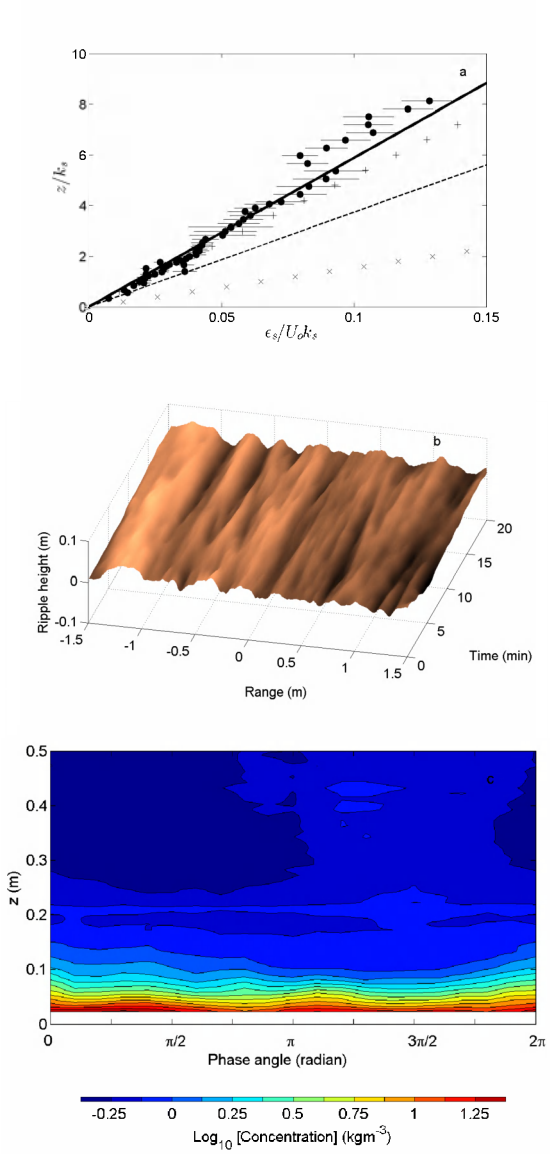

Figure 8 a) Comparison of the mean measured normalised sediment diffusivity (●) over the fine bed, with the predictions from equations (10) (– –), (8) (x,+ see text) and (11) (▬). b) A transect of the bed over time for an experimental run with H=0.79 m T=5s and c) variation in concentration with the phase of the wave and height above the fine bed.

These dimensions were typical of all the experiments, with $\langle\eta_r\rangle$=0.027±0.02 m, $\langle\lambda_r\rangle$=0.37±0.25 m, $\langle\eta_r/\lambda_r\rangle$= 0.07±0.01 and $\langle k_s\rangle$=0.05±0.03 m. For this range of slopes little significant flow separation or vortex formation is expected to occur (e.g. Sleath 1984).

Therefore, although the ripples enhanced the bed roughness somewhat, they acted on the flow dynamically like a plane bed. The equivalent roughness of the bed, if based upon $k_s=25\eta_r(\eta_r/\lambda_r)$, was just over a quarter that of that in the medium sand case, indicating that the impact of the bed on the flow is restricted to a region much closer to the bed than for the medium sand.

To assess the impact of ripples of low slope on sediment entrainment, the variation of the suspended sediment with the phase of the wave and the height above the bed for the fine sand was examined. An example of the results is shown in figure 8c for H=0.82 m and T=5s. The structure of the intra-wave suspended sediments is seen to be quite different from that shown in figure 7c; there are no significant suspension events near flow reversal lifting sediment well up into the water column. High concentrations are confined to a relatively thin layer within a few centimetres of the bed and the variation in the suspended load seems to be only weakly dependent on the phase of the wave, with only marginal increases in suspended concentration levels at maximum flow speed. The results in figure 8c indicate that the bed is behaving dynamically more like a plane bed, rather than a bed that is inducing vortex formation and entrainment. Therefore, the lack of a constant sediment diffusivity region in the fine sand case is not surprising, since the conditions for vortex entrainment were not present and it is the formation of vortices which are considered to be the underlying process leading to the constant sediment diffusivity region. For the fine sand case it is considered that the dynamics are comparable with the classical flat bed situation and that turbulent processes dominate the near-bed sediment entrainment. In this case the turbulent eddies are considered to grow with height above the bed (Davies and Villaret, 1997), leading to the linear increase in sediment diffusivity measured in this study over the bottom quarter of the water column.

4. CONCLUSIONS

Acoustics is now being used to measure, bedforms, suspended sediment, bedload, and hydrodynamics. The aim of the present paper was to describe and illustrate the use of acoustics in boundary layer sediment transport process studies. An example of the application of acoustic measurements has been

presented on sediment diffusivity profiles and comparisons made with three standard models and suggested new formulations have been presents. The work has shown how acoustics can be used to provide insight into understanding fundamental mechanisms of sediment processes

5. ACKNOWLEDGMENT

The work was supported by the EU contract MAS3-CT97-0106 and by the NERC, UK. The author is grateful to Professor Alan G Davies and Dr Paul S Bell for contributions to this work. Further details on this application of acoustics to sediment diffusivity studies can be found in Thorne, Davies and Bell (2009).

6. REFERENCES

Davies A.G. and C. Villaret, 1997. Oscillatory flow over rippled beds: Boundary layer structure and wave-induced Eulerian drift. Chapter 6 in Gravity Waves in Water of Finite Depth, ed. J.N. Hunt, Advances in Fluid Mechanics, Computational Mechanics Publications, 215-254.

Davies A.G. and Thorne P.D. 2005. Modelling and measurement of sediment transport by waves in the vortex ripple regime. Journal of Geophysical Research. Vol 110, C05017, doi:1029/2004JC002468, 2005. pp25.

Hay, A.E., Wilson, D., 1994. Rotary sidescan images of nearshore bedform evolution during a storm. Marine Geo. 119, 57-65.

Hay A.E., Zedel L., Cheel R. and Dillon J., 2012. On the vertical and temporal structure of flow and stress within the turbulent oscillatory boundary layer above evolving beds. Continental Shelf Research, 46, 31-49.

Hurther, D. and Lemmin U. (2008). Improved turbulence profiling with field adapted acoustic Doppler velocimeters using a bi-frequency Doppler noise suppression method. *J. Atmos. Oceanic Technol.*, 25 (2), 452-463.

Hurther, D, Thorne, PD and Bricault M, Lemmin U and Baroud JM. 2011. A multi-frequency acoustic concentration and velocity profiler (ACVP) for boundary layer measurements of fine-scale flow and sediment transport processes. Coastal Engineering. 58, 294-605 doi: 10.1016/j.coastaleng.2011.01.006.

Moate BD and Thorne PD. 2012. Interpreting acoustic backscatter from suspended sediments of different and mixed mineralogical composition. Continental Shelf Research, 46, 67-82.

Nielsen P. 1992. Coastal Bottom Boundary Layers and Sediment Transport. Advanced series on ocean engineering, volume 4. World Scientific, Singapore, 324 pp.

O'Hara Murray, R.B., Thorne, PD and Hodgson DM. 2011. Intrawave observations of sediment entrainment processes above sand ripples under irregular waves, J. Geophys. Res., 116, C01001, doi:10.1029/2010JC006216.

O' Hara Murray, Hodgson D.M and Thorne P.D. 2012. Wave groups and the character of sediment resuspension over an evolving sandy bedforms. Continental Shelf Research, 46, 16-30.

Ranasoma, K.I.M., and . Sleath J.F.A. 1992. Velocity measurements close to rippled beds, in Proceedings of the 23rd International Conference on Coastal Engineering, pp. 2383-2396, American Society of Civil Engineers, Venice, Italy.

Sleath J.F.A. 1982. The suspension of sand by waves. J. of Hydraulic Research, 20, 5, 439-452.

Soulsby R.L. 1997 Dynamics of marine sands. Thomas Telford publication, UK. 249 pp.

Thorne, P.D., Davies, A.G. and Bell P.S. 2009. Observations and analysis of sediment diffusivity profiles over sandy rippled beds under waves, J. Geophys. Res., 114, C02023, doi:10.1029/2008JC004944.

Thorne P.D., Hurther D. and Moate B.D. 2011. Acoustic inversions for measuring boundary layer suspended sediment processes. J Acoust Soc Amer 130(3) 1188-1200.

Traykovski, P. (2007). Observation of wave orbital scale ripples and a nonequilibrium time-dependent model. J. Geophys. Res. 112, C06026, doi:10.1029/2006JC003811

van der Werf J.J. Ribberink, J.S, O'Donoghue T and Doucette J.S. 2006. Modelling and measurement of sand transport processes over full-scale ripples in oscillatory flow. Coastal Engineering, 53, 657-673

Van Rijn L.C., 1993 Principles of sediment transport in rivers, estuaries and coastal seas. Aqua publications, the Netherlands. 633 pp.